J. exp. Biol. **137**, 421–442 (1988)
Printed in Great Britain © *The Company of Biologists Limited 1988*

THE FORCES ACTING ON SWIMMING SQUID

BY R. K. O'DOR

Biology Department, Dalhousie University, Halifax, Nova Scotia, Canada B3H 4J1

Accepted 23 February 1988

Summary

1. Analysis of ciné films and intramantle pressure records for squid *Loligo opalescens* Berry swimming in a tunnel respirometer provided estimates of all the forces acting in the horizontal and vertical planes for swimming speeds from 0·1 to 0·5 $m s^{-1}$.

2. Different speeds used different gaits; fin thrust was only important below 0·2 $m s^{-1}$, 'anaerobic' circular muscles were recruited only at supracritical speeds, and hyperinflation caused by contraction of the radial muscle was not seen in steady swimming.

3. The extent, rate and frequency of contraction of the obliquely striated circular muscles varied little with speed, and jet thrust was matched to speed primarily by active pressure control through adjustments in the size of the funnel orifice.

4. Hydrodynamic lift production to compensate for negative buoyancy during enforced horizontal swimming in the tunnel required 30–90 % of the total force over the speed range studied and appears less efficient than direct use of jet thrust. This suggests a new rationale for 'climb-and-glide' swimming which reduces previous estimates of the gross cost of transport for squid under natural conditions by at least 35 %, with no loss of speed.

5. The cost of accelerating water into the mantle of a squid moving at high speed appears to have been underestimated in previous studies. A simulation of a series of escape jets predicts a maximum speed of 8 body lengths s^{-1} (1·4 $m s^{-1}$), reached after only two jets, because of the high deceleration during refilling.

Introduction

Squid, which are the only truly nektonic invertebrates, live and compete in the open ocean with fishes and mammals using a propulsion system totally unlike that of their predators and competitors. Much has been written about undulatory and oscillatory swimming in fish (Gray, 1933; reviews by Webb, 1978; Magnuson, 1978; Blake, 1983), but the fundamental complexity of the interactions of body movements with propulsive and drag forces still defies complete description. In contrast, jet propulsion systems, which appear to be inherently simpler, received

Key words: *Loligo opalescens*, *Illex illecebrosus*, hydrodynamics, climb-and-glide, jet propulsion, negative buoyancy.

attention much more recently (Bradbury & Aldrich, 1969; Packard, 1969; Ward & Wainwright, 1972; see review by O'Dor & Webber, 1986). Squid actually use a combination of fin undulations and a jet which can direct thrust at any angle through a hemisphere below the body plane (Zuev, 1968), and their complete range of locomotory behaviour rivals that of reef fishes. This report will not attempt analysis of all modes, but will focus on 'backward' swimming with the fins first and the head behind, the most common mode and the way squid have been studied in swim-tunnels (O'Dor, 1982; Freadman *et al.* 1984; Webber & O'Dor, 1986). Swim-tunnel studies have dealt only with empirical observations on speed–oxygen consumption and speed–pressure relationships, and the only previous analytical approach to squid motion was a largely theoretical one (Johnson *et al.* 1972), based on the pressures and thrusts produced by tethered squid (Trueman & Packard, 1968). The present study includes intramantle pressure data and a kinematic analysis of ciné films of squid, *Loligo opalescens*, used in earlier swim-tunnel work (O'Dor, 1982). The analysis of this more complete data set indicates that most of the assumptions in the earlier equations of motion (Johnson *et al.* 1972) were oversimplifications and that swim-tunnel costs of transport cannot be transferred directly to nature; predicted maximum speeds and transport costs at low speeds have both been overestimated.

Abbreviations

A	area of funnel orifice	F_i	inertial force
a	acceleration	F_r	refilling force
B	buoyant weight	*g*	gravitational constant
C	coefficients	L	lift
C_b	coefficient of body drag	l_a	arm length
C_d	coefficient of discharge	l_f	fin length
C_f	coefficient of fin drag	l_h	head length
C_i	coefficient of induced drag	l_m	mantle length
C_l	coefficient of lift drag	l_t	total length
C_p	coefficient of added pressure drag	M	squid mass
D	drag force	M_t	total mass
D_b	body drag	P	power
D_f	fin drag	p	instantaneous pressure
D_i	induced drag	$\bar{p}$	average pressure
D_p	added pressure drag	Q	flow rate through funnel
D_t	total drag	R_a	aspect ratio
d_s	squid density	R_b	Reynolds number, body
d_w	water density	R_f	Reynolds number, fins
E	Froude efficiency	r_f	funnel orifice radius
F	forces	r_m	greatest mantle radius
F_a	axial forces ($F_i+F_r+D_b+D_f$)	r_r	r_m at rest
F_b	balancing force	S	surface area

S_f	fin wetted surface area	T_{jh}	horizontal jet component
S_p	body planar surface area	T_{jv}	vertical jet component
S_w	body wetted surface area	t	frame interval
T	thrust	u	squid speed
T_f	fin thrust	u_c	current speed
T_h	horizontal components	u_j	jet velocity
T_j	jet thrust	V	total mantle volume
T_v	vertical components	V_w	mantle water volume
T_{fh}	horizontal fin component	x	mantle thickness
T_{fv}	vertical fin component	θ	angle of attack

Materials and methods

Oxygen consumptions for mature male *Loligo opalescens* during 1 h stages at increasing current speeds up to the maximum sustainable (critical) speed were determined in the original, 11·5 cm inside diameter, Brett (1964) tunnel respirometer as previously described (O'Dor, 1982) at Bamfield Marine Station in British Columbia. During these experiments, nine non-cannulated squid were filmed from above through a reference grid using a Minolta XL-500 Super-8 camera. Some segments also included side views taken with a mirror. Close-ups through a mirror beneath the swim-chamber allowed measurement of funnel orifice diameter at low speeds. Records of intramantle pressures for three squid were made using PE-160 cannulae (Webber & O'Dor, 1986), a Narco Telecare RP-1500i pressure transducer and an Omniscribe B-5000 recorder with an integrator. The principle data sets used in this analysis were from two squid with masses (M) 0·033 and 0·031 kg which yielded usable film and pressure records, respectively, for current speeds (u_c) of 0·1, 0·2, 0·3, 0·4 and 0·5 m s^{-1}.

After swim-tunnel tests the squid were anaesthetized in 2 % ethanol in sea water and standard morphometrics taken. Various body parts were also dissected out and weighed. To estimate the required lift, six squid were weighed on spring scales (Pesola, Switzerland) in air and in water to the nearest 0·1 or 0·05 g, respectively, prior to dissection.

Kinematics

Squid could swim at any set subcritical current speed, but swam less steadily than undulating fish, with most individuals first moving forward in the swim chamber for a few jet cycles and then falling back. To avoid errors caused by such drifting, 5–10 jet cycles with no net change in squid speed were chosen from the available film at each current speed and analysed frame by frame for characteristic changes in squid speed (u), greatest mantle radius (r_m) and fin position. The average speed from frame to frame was calculated from the change in position of a feature on the squid relative to the grid with a correction for the precalibrated current speed. The frame interval (t) of 0·0555 s was confirmed by filming a stopwatch. The frame with the lowest r_m in each cycle, indicating the end of the

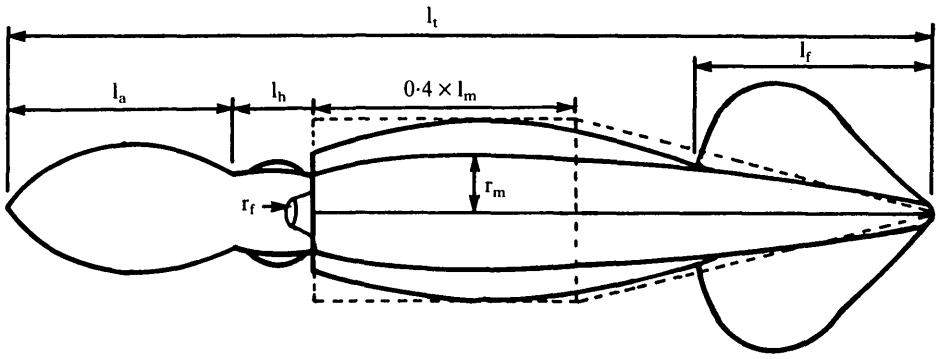

Fig. 1. Summary of the measurements used in the simulation, superimposed on tracings of a squid at maximum and minimum mantle volume. The lengths (l_a, arms; l_f, fins; l_h, head; l_m, mantle; l_t, total) are used to calculate surface areas and the radii (r_f, funnel orifice; r_m, maximum mantle radius) to calculate jet area (A) and mantle volume (V), respectively. The dashed lines outline the mantle component of the body planar surface area (S_p) actually used in a simulation at maximum mantle volume and suggest the equations used to calculate this variable.

contraction phase, was used as a reference to align the cycles, and average values for r_m and u were calculated for each subsequent frame. Maxima and minima were used directly, but running means of three points were used to smooth the curves between them (see Fig. 2) because of the large effect small deviations in distance have on second derivatives such as acceleration. These 'average' cycles were used for all further calculations. Analysis of the simultaneous incremental (frame-to-frame) changes in variables was made with an Apple IIc microcomputer with a Z-Ram Ultra 3 expansion card (Applied Engineering, Carrolton, Texas) using the spreadsheet from the Appleworks software package.

Because of the cyclic nature of jet propulsion, squid oscillated forwards and backwards in the swim-chamber and camera frame, making it impossible to obtain complete mantle profiles over entire cycles, but the point of maximum diameter was usually visible. A 0·135 m mantle length (l_m), 0·040 kg (M) squid filmed in top and side view yielded 15 frames with complete profiles during horizontal swimming with greatest radii (r_m) ranging from 0·0094 to 0·0160 m. Regression of r_m^2 against total mantle volume (V, m^3), calculated by assuming radial symmetry and treating mantle outlines (Fig. 1) as a series of 0·005 m long cylinders, yielded a correlation coefficient of 0·995 for $V = 0{\cdot}17r_m^2 + 0{\cdot}000009$. As Fig. 1 also shows, the back third of the mantle, which is enclosed by the pen, is essentially rigid, accounting for most of the volume which is independent of mantle radius. The volume of water in the mantle will equal V minus the volume of muscle and viscera. When the mantle is at rest with a greatest radius (r_r) of 0·015 m its thickness (x) is 0·002 m, giving a muscle volume of 0·0000096 m^3, and, at minimum r_m, the residual volume is 0·0000152 m^3. The visceral volume for this squid was 0·0000103 m^3 and, assuming that the invariant volume component consists of one third of the muscle plus viscera, this leaves 0·0000045 m^3 of viscera in the active

mantle. For ease of calculation and to allow for scaling, it was convenient to use an equation for mantle water volume, V_w, which treats the mantle as a single cylinder of changing diameter with a length less than the total mantle length (compensating for non-uniform contraction) and includes corrections for mantle muscle and viscera:

$$V_w = [r_m{}^2 - (r_r - x)^2]\,(0{\cdot}4\pi l_m) - (0{\cdot}12M/d_s)\,. \quad (1)$$

This equation closely approximates the variable component of the regression and makes a reasonable correction for visceral mass based on mantle length, resting mantle radius and thickness and the mass of the squid as measured at death, using a squid density, d_s, of $1055\,kg\,m^{-3}$ (see Results). At best, V_w can only be an approximation since reproductive stage and even stomach or bladder contents will influence it. For the standard squid ($M = 0{\cdot}032\,kg$; $l_m = 0{\cdot}121\,m$; total length, $l_t = 1{\cdot}5l_m = 0{\cdot}182\,m$), V_w is $0{\cdot}0000176\,m^3$ at $r_r = 0{\cdot}0138\,m$, $x = 0{\cdot}002\,m$. All these values are consistent with those used by Gosline & Shadwick (1983) in their analysis of escape jets in *L. opalescens*.

Hydrodynamics

To clarify the forces acting on the squid in various parts of the cycle, standard rigid-body equations were used as a first approximation to calculate lift and drag forces, F, at various speeds, u.

$$F = 0{\cdot}5d_w u^2 SC\,, \quad (2)$$

where S is surface area and C is a drag or lift coefficient. The density of sea water (d_w) was taken as $1023\,kg\,m^{-3}$. The planar surface area (S_p) was taken as the sum of the head and arm areas taken from tracings and equal to $0{\cdot}11\,l_m{}^2$ plus a variable component calculated as the area of a rectangle $2r_m$ by $0{\cdot}4l_m$ and the attached triangle $0{\cdot}6l_m$ high as indicated in Fig. 1. Frictional drag on the body (D_b) was calculated using wetted surface area ($S_w = \pi S_p$) and a drag coefficient for laminar flow ($C = 1{\cdot}33/R_b{}^{0{\cdot}5}$) corrected for pressure drag on a streamlined body to:

$$C_b = C[1 + 1{\cdot}5(2r_m/l_t)^{1{\cdot}5} + 7(r_m/l_t)^3] \quad (3)$$

(where C_b is body drag), as discussed by Blake (1983). The Reynolds number for the body was taken as $R_b = ul_t \times 10^6$, where l_t is the total body length. The fins, at the leading edge, were treated as a separate flat plate oriented parallel to the flow, and minimal fin drag (D_f) was estimated using equation 2 with the wetted surface area from tracings ($S_f = 0{\cdot}36l_m{}^2$) and fin drag coefficient, C_f, calculated like C above using a Reynolds number, R_f, based on the length of the fins ($l_f = 0{\cdot}4l_m$).

Since the squid increased their angle of attack, θ, at lower speeds as indicated in Fig. 5 (see Results), additional pressure drag (D_p) and lift (L) forces were calculated using equation 2 with coefficients based on the cross-flow principle, treating the squid as cylinders with changing angles relative to the flow (Hoerner, 1965). The coefficient of added pressure drag, C_p, is $1{\cdot}1\sin^3\theta$ and the coefficient of lift, C_l, is $1{\cdot}1\sin^2\theta\cos\theta$. Induced drag ($D_i$) was similarly calculated using $C_i = C_l{}^2/\pi R_a$, where the aspect ratio (R_a) is 0·6.

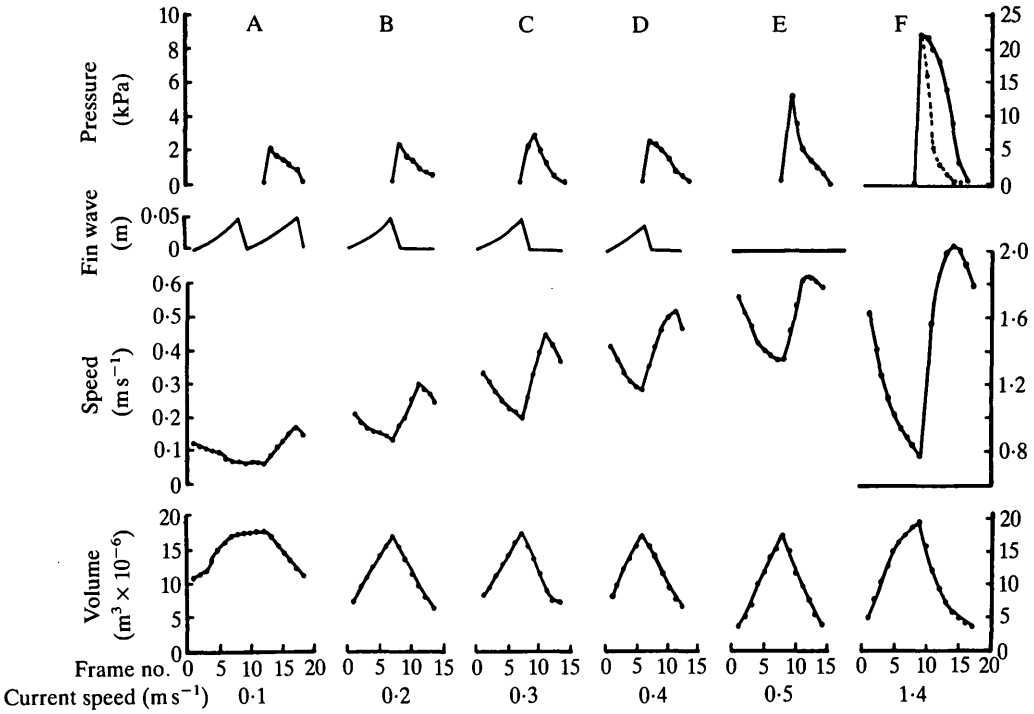

Fig. 2. Summary of cyclic changes in critical variables at various speeds as determined from frame-by-frame analysis and pressure records. F is based on escape jet mantle radius and pressure (solid line) data from Gosline & Shadwick (1983); volumes are calculated from radius changes, speeds are predicted by simulation, and the dashed line is the pressure calculated using a constant funnel radius (see Fig. 4). For the simulation in F, the data were scaled to the size of a 'standard' squid and the duration of the refilling phase in a series of continuous escape jets was estimated from pressure records.

Results

Gaits

Fig. 2 summarizes the changes in the locomotor cycles of a squid swimming against increasing current speeds as indicated by the squid speed (u), the volume of water in the mantle (V_w), and the position of the trailing edge of the fin wave as it moved from the tip of the mantle towards the head. These patterns reveal several unexpected features of squid swimming. At all tested speeds, the duration of the contractile phase was constant, but the length of the refilling phase decreased gradually until the squid reached their maximum sustainable or 'critical' speed of about $0{\cdot}4\,m\,s^{-1}$ (O'Dor, 1982). Below $0{\cdot}2\,m\,s^{-1}$ the fins produced two waves for each mantle contraction, but at higher subcritical speeds a single wave per cycle occurred during refilling. Above the critical speed, the fins were rolled tightly against the mantle and appeared to play no role. The pattern of mantle contraction also changed with speed in four distinct steps consistent with the use of collagen 'springs' in the mantle to power refilling (Gosline & Shadwick, 1983). At

$0{\cdot}1\,m\,s^{-1}$, the amplitude of the contraction is small, suggesting that distortion of the springs is minimal and that the mantle stores little energy. As a consequence, refilling is slow and nearly all muscle work is used to pressurize the jet. The volume changes at the three intermediate speeds are very similar and large enough for the springs to store significant energy. However, the same amount of refilling occurs progressively faster, and it remains unclear how the increasing power required to refill in shorter times at higher speeds is supplied. Vogel (1987) has shown that the 'Bernoulli effect' related to negative pressures produced by the increased speed of the water flowing over the outside of the mantle is a factor only at high speeds. At $0{\cdot}5\,m\,s^{-1}$, the amplitude of contraction is maximal, and the full capacity of the springs is available to power more rapid refilling. The principle differences between escape jets (Fig. 2F) and supracritical speed jets appear to be a greater maximum diameter, presumably produced by active expansion resulting from radial muscle contractions, and a slightly longer contractile phase stemming from the increased shortening required.

These results indicate that squid swim at continuously variable speeds using the complex interaction of several muscle systems to produce at least four different 'gaits' which allow them to use the particular locomotor elements giving the greatest efficiency at a given speed. Squid have difficulty maintaining a precise speed, but 'typical' cycles at a given speed can be simulated by choosing cycles that begin and end at the same speed. Even such cycles are not identical, presumably because of small changes in drag due to the angle of attack. The average standard errors for all averaged mantle diameters and speeds in the frame-by-frame analysis used to construct Fig. 2 were 1·6 % and 5·3 %, respectively. The error generally increased with increasing speed, ranging from 0·3 % at $0{\cdot}1\,m\,s^{-1}$ to 4·2 % at $0{\cdot}5\,m\,s^{-1}$ for diameter and from 4·0 % at $0{\cdot}1\,m\,s^{-1}$ to 7·8 % at $0{\cdot}5\,m\,s^{-1}$ for speed. The analysis that follows is an attempt to understand this optimization, using the data from Fig. 2 to predict the forces acting on a squid at various speeds. These cycles clearly are not the only way a squid can swim, but should be representative.

Force balance

Daniel (1983, 1985) described the force balance over the jet cycle of medusae with a single equation and provided numerical solutions. The forces acting on squid vary with the gait and the phase of the cycle to such an extent that no continuous function seemed likely to describe them adequately. The present analysis looks at each frame in a cycle as a discrete increment, balances the forces in both the vertical and horizontal planes, and then calculates the average forces acting over a cycle at a speed to simulate various gaits. The overall balance can be expressed in two equations summarizing the vertical and horizontal forces separately as shown in Fig. 3B. Parameters outlined below were adjusted so that vertical components always equal the buoyant weight, B. Based on a water/air weight ratio of $0{\cdot}033 \pm 0{\cdot}002$ for six squid; $B = 0{\cdot}033\,Mg = 0{\cdot}0107$ N for a 0·032 kg squid and:

$$B = T_{jv} + T_{fv} + L\,, \tag{4}$$

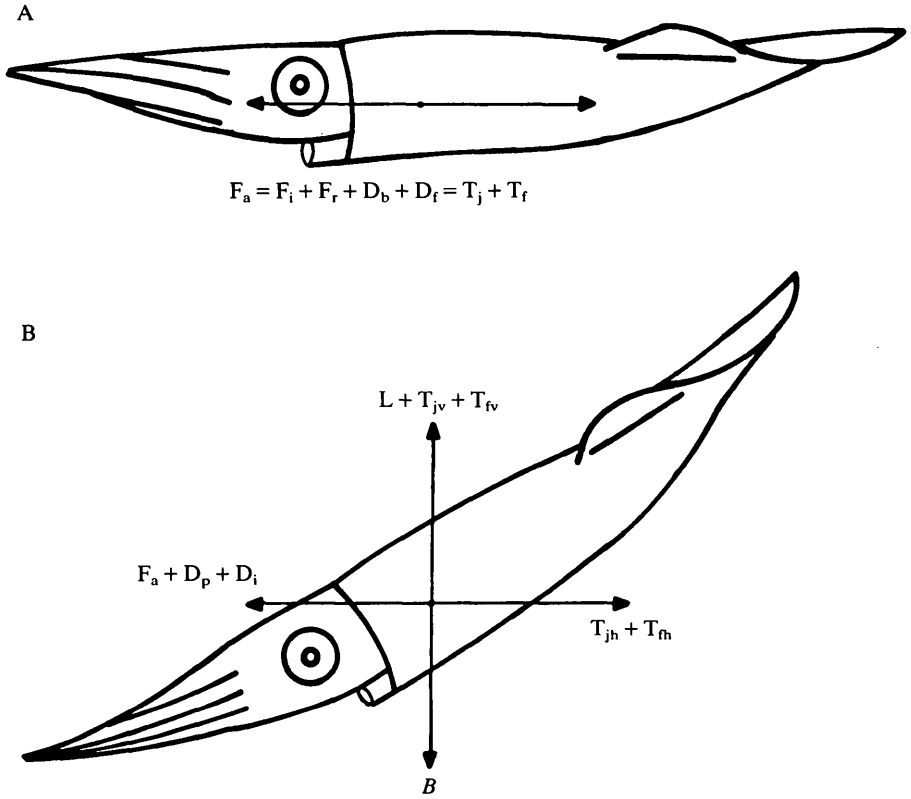

Fig. 3. (A) Summary of the forces acting on a theoretical, neutrally buoyant squid moving with its body axis parallel to the flow. Jet, T_j, and fin, T_f, thrust act against axial forces F_a (the sum of body, D_b, and fin, D_f, drag and inertial, F_i, and refilling, F_r, forces). (B) Real squid use a combination of thrust and lift, L, produced by cross-flow to counter their buoyant weight, *B*, in horizontal swimming. The positive angle of attack required to produce lift also produces added pressure drag, D_p, and induced drag, D_i.

where T_{jv} and T_{fv} are the vertical components of jet and fin thrust, respectively, and L is the lift. The calculated horizontal components should also sum to zero (forces in the direction of current flow are considered positive), but the imbalance (F_b) is calculated to indicate the direction and magnitude of the errors in estimates using the equation:

$$F_b = T_{jh} + T_{fh} + F_r + F_i + D_b + D_f + D_i + D_p \,, \qquad (5)$$

where T_{jh} and T_{fh} are the horizontal components of jet and fin thrust, F_i is the inertial force related to acceleration or deceleration of the squid and the water it contains, and F_r is the force required to accelerate water entering the mantle during refilling to the speed of the squid. The various drag forces (D) are defined in Materials and methods. Thrust produced by fin undulations (T_f) only appears to be significant at low speeds, as discussed below.

The intake and expulsion of water by the mantle are important at all speeds and

are much more complex than in medusae, where Daniel (1983) assumes the velar aperture to be constant in both phases. In squid there is an estimated 20-fold change in orifice size between refilling (phase 1), through the entire mantle opening, and jetting (phase 2), through the much smaller funnel orifice (Trueman, 1980). Daniel considered that the two phases simply produced thrust in opposite directions, but, because of the large difference in squid, a separate term is used to distinguish the large negative (against the current) jet thrust (T_j), which has been divided into vertical and horizontal components, from the positive jet thrust or refilling force (F_r), which has not. As Daniel (1984) indicates, the acceleration reaction averages to zero over a cycle, and is probably not a major factor in squid swimming at higher speeds. For simplicity, the present calculations assume an added-mass coefficient of zero, which should produce no errors in comparisons between cycles and only small errors in calculations within a cycle (e.g. Fig. 6). Treating a squid as an ellipsoid moving parallel to its long axis predicts added-mass coefficients of between 0·024 and 0·040 as the fineness ratio varies from 9·0 to 6·4 over the cycle (Daniel, 1985; Lamb, 1962), and the true value is probably not much greater. During phase 2, the jet thrust, T_{jh}, initially exceeds total drag force (D_t; the sum of frictional drag on body, D_b, and fins, D_f, the added pressure drag, D_p, and induced drag, D_i), producing accelerations, a. The inertial force, F_i, must equal $M_t a$, where total mass $M_t = M+V_w d_w$. Accelerations are not reported directly but are readily derived from the speed data in Fig. 2. When T_{jh} drops below D_t, deceleration begins, and F_i becomes negative. In phase 1, the inertial force from deceleration must overcome drag, accelerate refilling water and provide lift.

The values for the forces at each speed were calculated in the following order.

(1) Pressures in each frame were calculated (equation 10, below) by converting volume changes from Fig. 2 to flow rates. A funnel radius was assumed which gave an average pressure over the cycle equal to that calculated by regression. Jet thrust was then calculated from pressure (equation 6, below).

(2) Two minimum attack angles were selected to give lift greater than buoyant weight in phase 1 and lift plus vertical jet thrust greater than buoyant weight in phase 2.

(3) The other forces (F_i, F_r, D_b+D_f and D_p+D_i) were calculated for each frame from greatest mantle radius, speed and attack angle.

(4) The forces from 3 were summed with horizontal jet thrust to estimate the balancing force (equation 4) for each frame.

The details of and rationale for key individual calculations follow.

Jet thrust from pressure

The most important force in phase 2 is jet thrust, which Johnson *et al.* (1972) calculated as:

$$T_j = 2C_d A p \,, \qquad (6)$$

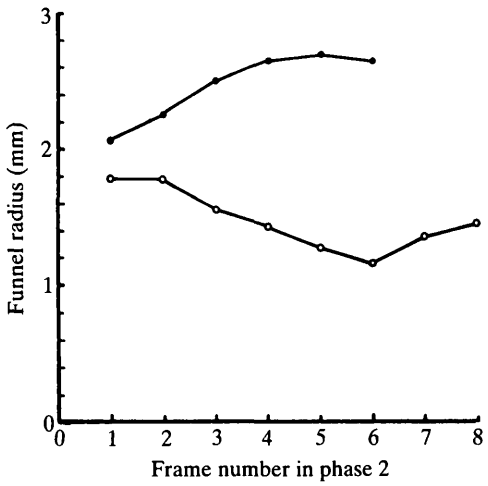

Fig. 4. A comparison of the cyclic changes in measured funnel radius at $0{\cdot}2\,m\,s^{-1}$ (filled circles) with the calculated funnel radii needed to produce the measured pressures during an escape jet (open circles).

from known pressures (p), assuming a constant area (A) for the funnel orifice. They found that a coefficient of discharge (C_d) of about 0·6 was required for a reasonable relationship between measured pressures and thrusts. However, films of the funnel orifice at $0{\cdot}2\,m\,s^{-1}$ confirmed Zuev's (1968) observations that the funnel orifice varies over the cycle. Fig. 4 plots the measured funnel radius (r_f) over the six frames of phase 2; funnel radii were synchronized to frames in the cycle using simultaneously measured speeds. These variations probably contribute to the low C_d inferred by Johnson *et al.* (1972) but could not be determined accurately at higher speeds where close-up filming was impossible. Knowing the exact area is unnecessary in the present analysis, however, since the flow rate through the funnel can be calculated as:

$$Q = \Delta V_w / t \,, \tag{7}$$

where t is the frame interval. The jet velocity, u_j, could alternatively be calculated from the Bernoulli equation as:

$$u_j = (2p/d_w)^{0{\cdot}5} \,, \tag{8}$$

and jet thrust as:

$$T_j = d_w Q u_j \,. \tag{9}$$

Unfortunately, the recording techniques used did not allow exact synchronization of film frames with pressure records, and the slow mechanical response of the pens underestimated peak pressures. However, the electronic integrator gave reliable average pressures ($\bar{p}$) which could be reconstructed from incremental changes and

are convenient for comparison with other work (Webber & O'Dor, 1986). In practice, since $u_j = Q/A$, equation 8 was rearranged as:

$$p = 0{\cdot}5d_w(Q/A)^2 , \quad (10)$$

and values of A (assuming $A = \pi r_f^2$) were determined which gave values of $\bar{p}$ over the cycle equal to those measured for squid at each speed (see below). The areas calculated in this way are effectively the areas of the jet itself, rather than the orifice, and a C_d of 1·0 was used to calculate jet thrust from equation 6. It should be noted that equations 6 and 9 are both based on an assumption of constant u_j and ignore the force produced by the changing speed of the mass of water in the jet which previous workers assumed to be negligible. Estimates of this component from calculated frame-to-frame changes in u_j confirm that they were correct; the thrust due to changing velocity contributed only 0·5–1·0 % of the total thrust over the speed range.

Constant funnel radii yielded pressures for individual frames which rose much more slowly over the cycle than actual pressure records (data not shown) which were known to be too slow because of the recording technique. The values in Table 1 were calculated by adjusting the maximum funnel radius at each speed while maintaining the same relative funnel radius from frame to frame as was measured at $0{\cdot}2\,m\,s^{-1}$ (Fig. 4). This pattern of increasing funnel radius during the early stages of mantle contraction gave the more typical curves shown in Fig. 2. Fig. 2 also compares a similarly calculated curve based on mantle radii for restrained *L. opalescens* during apparent escape responses from Gosline & Shadwick (1983) with their actual synchronous pressure data. Fig. 4 shows the pattern of funnel radius changes required to generate the measured pressures, given the flow rates calculated from measured mantle radius changes.

The changing pattern of funnel radii indicates dynamic muscular control of the orifice. At low speeds, funnel muscles appear to relax during mantle contraction, but at high speeds they continue to contract through most of the cycle. If this activity is fully graded, there is presumably some intermediate speed at which the funnel radius remains nearly constant. Fortunately, the pattern of orifice change is less important to thrust production than the average magnitude of the funnel radius. Comparing the thrust produced by a constant funnel radius pattern with that produced by the $0{\cdot}2\,m\,s^{-1}$ and escape jet patterns, using the $0{\cdot}5\,m\,s^{-1}$ data, gives changes of only 3 and 20 %, respectively, when the maximum funnel radius is adjusted to produce the same average pressure. If the same maximum funnel radius is used in all three patterns, the increases are 30 and 85 %, respectively. Thus, matching the *pattern* of orifice changes at a speed is less critical than matching the average funnel radius.

Average pressures are available for only three *L. opalescens* at 15 speeds, but the pattern is consistent with similar results for *Illex illecebrosus* weighing about 10 times more (Webber & O'Dor, 1986). A regression of $\ln \bar{p}$ (Pa) *versus* u ($m\,s^{-1}$) gave the relationship, $\bar{p} = 127e^{4{\cdot}9u}$, with a correlation coefficient of 0·975. This can be compared to $\bar{p} = 350e^{2{\cdot}1u}$ for *I. illecebrosus*, which Webber & O'Dor found to

Table 1. *Summary of the average forces and other variables affecting squid at various speeds in a swim-tunnel*

	Current speed u_c ($m\,s^{-1}$)					
	0·1	0·2	0·3	0·4	0·5	1·4
Inertial force, F_i	0·0001	0·0009	0·0012	0·0014	0·0020	0·0056
Refilling force, F_r	0·0007	0·0025	0·0038	0·0056	0·0077	0·0203
Body and fin drag, D_b+D_f	0·0012	0·0034	0·0066	0·0094	0·0130	0·0642
Total axial forces, F_a	0·0020	0·0068	0·0116	0·0164	0·0227	0·0901
Lift drag, D_p+D_i	0·0050	0·0060	0·0031	0·0024	0·0020	0·0011
Loligo regression						
Horizontal thrust, T_h	−0·0103*	−0·0148	−0·0189	−0·0251	−0·0387	
Force imbalance, F_b	−0·0029	−0·0021	−0·0043	−0·0063	−0·0141	
Illex regression						
Horizontal thrust, T_h	−0·0130*	−0·0187	−0·0208	−0·0240	−0·0320	−0·0971
Force imbalance, F_b	−0·0060	−0·0060	−0·0062	−0·0052	−0·0073	−0·0061
Frequency (s^{-1})	1·00	1·33	1·39	1·50	1·29	1·06
Average pressure, $\bar{p}$ (Pa)	430	530	660	820	1000	6370
Funnel radius, r_f (m)	0·0024	0·0029	0·0028	0·0027	0·0028	0·0018
Refilling angle, θ (degrees)	38	28	16	13	10	5
Jetting angle, θ (degrees)	13	10	8	7	5	2
Froude efficiency	0·12	0·22	0·26	0·31	0·31	0·34

* Includes T_f from fins of 38 and 25 %, respectively, for the two pressure–speed regressions.

Negative forces (given in newtons, N) act in the direction of motion.

Two different regressions of pressure *versus* speed were tested in the model; the one based on data from *Loligo* was not used in the final analysis because the increasing force imbalance with speed indicated a large artefact from pressure cannula drag in these small animals (see text).

be relatively insensitive to squid mass. The higher exponential coefficient in the smaller squid appears to be a measurement artefact as discussed in the analysis below.

Refilling

In phase 2 large positive pressures in the mantle force water through the funnel at high velocity producing jet thrust, but in phase 1 much smaller negative pressures inside the mantle (Trueman, 1980; Gosline *et al.* 1983; Webber & O'Dor, 1986) produce a reverse jet (into the mantle) which must have a velocity at least equal to the squid's speed. Precise calculation of refilling force, analogous to that of jet thrust, might be possible if negative pressures and mantle orifice areas could be measured (Trueman, 1980), but reasonable estimates are possible without such details. The water flow into the mantle, Q, producing the incremental increase in volume between frames, must be accelerated from a relative speed of zero to that of the squid in the frame interval, and a minimum force, $F_r = d_w Qu$, must be exerted. This force is the product of mass and acceleration and is analogous to equation 9. If the orifice of the mantle is adjusted appropriately, the intake jet velocity should just equal the speed of the squid, allowing water to flow into the mantle with little wasted energy. Such adjustments may occur automatically, since the lip of the mantle is closed against the head at the end of phase 2, and this 'seal' will be influenced by the developing negative pressure in the mantle. The mantle lip can be opened under muscular control (Gosline & DeMont, 1985), but flow can only occur when the combination of pressure and orifice area produce a u_j equal to u. If there is not enough pressure, no refilling will occur until the squid slows down. This is consistent with the pattern of increasingly negative pressures with increasing speeds seen in these experiments and reported for *I. illecebrosus* (Webber & O'Dor, 1986). Some of the energy used to accelerate refilling water early in the cycle will be recovered as this mass of water decelerates; this is accounted for by the incremental increase in mantle volume in later calculations of inertial force, F_i.

Lift and angle of attack

The last complication is that both thrust, T, and inertial force, F_i, must be divided into vertical and horizontal components. This depends on the orientation of the funnel and angle of attack (θ). Using their keeled arms and fins as control surfaces on opposite ends of the body and the funnel to produce directed thrust, squid can move in almost any direction they wish. One squid swam at two speeds with negative angles of attack but, as Fig. 5 shows, the limited data from side views confirms general observations (Zuev, 1968) that θ typically decreases from about 30° when hovering to near 0° at high speeds. A complete description of the forces in even the simplest mode would be very complex and require high-resolution side-view films. The simplifying assumption that jet thrust (and fin thrust, at low speeds) always acts parallel to the axis of the squid is probably rarely true, but it makes the calculations manageable ($T_v = T\sin\theta$, $T_h = T\cos\theta$; Hertel, 1966) and

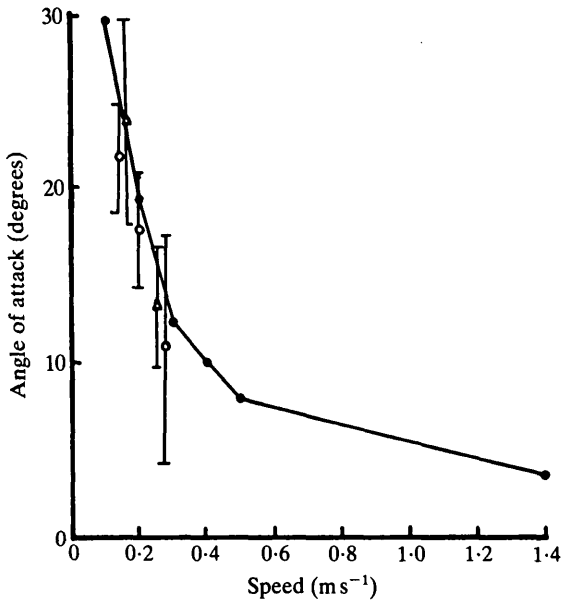

Fig. 5. Average angle of attack over a cycle required to produce the necessary lift at various speeds in the simulation (filled circles) compared with the means and standard deviations of measured angles in two squid (open symbols). Angles were measured for 10–20 frames over several cycles at each of five speeds.

gives results within a few degrees of the available observations. Since buoyant weight is constant and jet thrust is absent in phase 1, lift and attack angle should vary considerably between phases 1 and 2. In subsequent calculations, the minimum integer angle giving an average phase 1 lift, L, greater than the buoyant weight, B, was used throughout phase 1 and that giving $L+T_{jv}$ greater than B throughout phase 2. The calculated angles are given in Table 1. As expected, the angle varies dramatically between phases, particularly at low speeds because of the varying contribution of the jet. Some angular variation does occur in real squid over the cycle, but probably not as much as the calculations suggest, presumably because the squid make constant corrections with control surfaces. The values plotted in Fig. 5 are time-weighted averages which seem to represent the real situation reasonably accurately.

Fins

At low speeds, the fins undulate continuously (Fig. 2) and probably produce thrust (T_f) almost continuously, but a detailed analysis of fin activity would again require high-resolution side views. The limited data from top views in Fig. 2 show, however, that the wave moves along the fin at a relatively constant speed, clearly less than $0{\cdot}15\,m\,s^{-1}$, regardless of swimming speed. Since the speed of the undulatory wave must exceed the animal speed to produce thrust (Gray, 1933), fin thrust was ignored in the analysis of speeds above $0{\cdot}1\,m\,s^{-1}$. Decreasing periods of fin activity at higher speeds indicate a reduced role for the fins and, although they

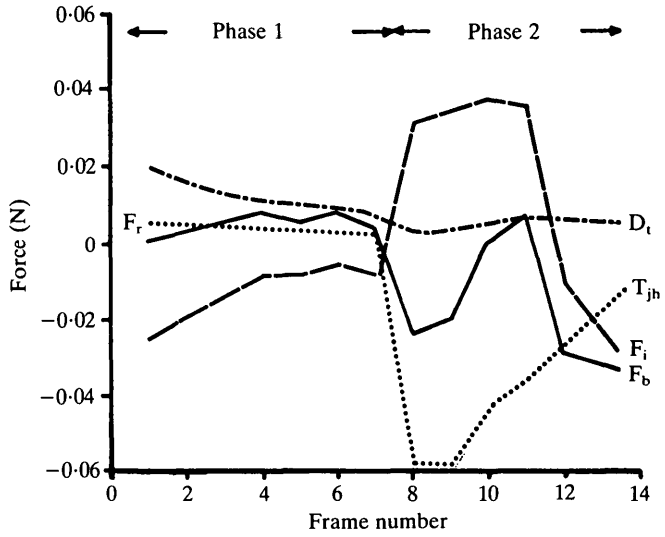

Fig. 6. Calculated forces for each frame interval over a jet cycle at $0{\cdot}2\,m\,s^{-1}$, assuming instantaneous changes in angle of attack between phases. The dotted line indicates the refilling force, F_r, in phase 1 and the horizontal component of jet thrust, T_{jh}, in phase 2. The uneven dashed line is the sum of the drag forces, D_t, and the even dashed line is the inertial force, F_i. The solid line is the balance of all horizontal forces, F_b.

may generate some thrust during the refilling phase below $0{\cdot}3\,m\,s^{-1}$, their principle contribution is probably in attitude control. At $0{\cdot}1\,m\,s^{-1}$ calculated jet thrusts (see below) are not high enough to balance even the buoyant weight over the cycle, indicating that the fins must be contributing thrust at this speed. Since there are three frames in phase 1 at $0{\cdot}1\,m\,s^{-1}$ with no change in speed or volume (Fig. 2), the net fin thrust during this period should equal the sum of the drag forces, calculated as 0·0039 N. The values for $0{\cdot}1\,m\,s^{-1}$ in Table 1 assume that this force was applied in all frames, since the fins were continuously active at this speed, and was divided into vertical and horizontal components on the same basis as jet thrust. The power output (calculated as $P = T_f u$) is reasonable, being approximately equal to that calculated for undulating fins of similar size in fish (Blake, 1980). The actual force may be larger but offset by the augmented drag associated with undulations, as is thought to occur in fish (Blake, 1983). There is no obvious way to calculate the augmentation factor from available data, but there is scope for added drag in the force balance at those higher speeds where fins are active. Some contribution from fin thrust late in phase 1 at $0{\cdot}2\,m\,s^{-1}$ is also possible, as discussed above, and would improve the balance as shown in Fig. 6. However, Table 1 assumes $T_f = 0$ at speeds above $0{\cdot}1\,m\,s^{-1}$.

Distribution of forces

Table 1 first gives the average value over the cycle for each force and for the balance using the pressure *vs* speed regression for *L. opalescens* to calculate jet

Table 2. *Distribution of forces as a percentage of the sum of the horizontal and vertical force components at various speeds*

	Current speed ($m s^{-1}$)					
	0·1	0·2	0·3	0·4	0·5	1·4
Lift A ($B+D_p+D_i-F_b$)	91	76	63	53	47	16
Lift B ($B+D_p+D_i$)	66	57	44	38	30	11
Drag (D_b+D_f)	5	12	21	27	30	60
Refilling (F_r)	3	9	12	16	18	19
Net inertia (F_i)	1	3	4	4	5	5

thrust (equation 6). As speed increases, the balance becomes progressively more negative, suggesting either that drag is much higher than the rigid body equations predict or that calculated jet thrusts are too high. The second set of sums in the Table, for jet thrusts calculated from the regression for *I. illecebrosus*, gives a more consistent picture, suggesting that the error is in the pressure data. Webber & O'Dor (1986) found that even in the much larger *I. illecebrosus* the use of cannulae to measure pressure appeared to increase the power required to swim at higher speeds. This is presumably due to the drag caused by the cannula, an effect which would be much more pronounced in smaller squid. The better balance from the *I. illecebrosus* regression is consistent with the view that the pressure–speed relationship has a low size-dependence.

The balance of forces for non-cannulated squid in phase 1, when jet thrust is not a factor, also indicates that the forces other than jet thrust are reasonably well balanced. As Fig. 6 shows, there is a slight excess of positive forces at $0{\cdot}2\,m\,s^{-1}$, but at higher speeds the inertial force usually balances the calculated positive forces. The net inertial force over the cycle is positive but small (Table 2), because of the water taken in during refilling. This is consistent with a low added-mass coefficient and a small acceleration reaction. However, a small added-mass of water carried with the squid would improve the force balance at the low speeds. The dramatic shifts in the balancing force in phase 2 of Fig. 6, for example, largely reflect the artificially abrupt change in attack angle, but would be smoothed by the accelerating and decelerating added-mass.

A test simulation

Given pressures and mantle radius changes over a cycle, the equations outlined above seem to predict the motion of a squid reasonably well. Reliable data is unavailable for squid swimming above $0{\cdot}5\,m\,s^{-1}$, but, if swimming in a series of escape jets produces a maximum speed, analysis of the escape cycle in Fig. 2F (from Gosline & Shadwick, 1983) should predict it. Because the end volumes of isolated escape jets are less than the starting volumes, the mantle radii during the last third of phase 1 have been adjusted to complete a cycle with a duration estimated from measurements of the time between normal pressure peaks when occasional high pressure jets were recorded. The speed profile in Fig. 2F was

generated by assuming that inertial force balanced all other forces, calculated as above, in each frame. The balancing force in Table 1 results from rounding speeds to the nearest $0{\cdot}001\,m\,s^{-1}$ and allowing the minimum negative surplus in each frame. Stepping through frames from $u = 0$ gives an acceleration curve which reaches $1{\cdot}6\,m\,s^{-1}$ (9 body lengths s^{-1}) on the first jet and stabilizes after the second at an average speed of $1{\cdot}4\,m\,s^{-1}$ with a cycle maximum of $2{\cdot}0\,m\,s^{-1}$. These should be upper limits since the Reynolds number exceeds 350 000 during the cycle, indicating that higher turbulent drag forces would apply. The highest speed ever observed in the swim-tunnel was $1{\cdot}05\,m\,s^{-1}$, but comparable speeds have been reported ($2{\cdot}1\,m\,s^{-1}$ or 10 body lengths s^{-1}; Packard, 1969) after a single jet in a *Loligo vulgaris* about 10 % longer. This maximum speed is lower than those attributed to squid anecdotally (Vogel, 1987) but is consistent with all direct observations as discussed by O'Dor (1982).

Discussion

This analysis was undertaken to resolve inconsistencies between the measured costs of locomotion of squid in swim-tunnels and the apparently lower costs predicted by earlier analyses (Johnson *et al.* 1972) and suggested by studies of squid in nature (O'Dor, 1988*a*). The most important factor relates to the negative buoyancy of the squid. In Table 2 the sum of calculated forces is partitioned among various activities. Maintenance of vertical position, including $-B$, D_p and D_i, requires at least 66 % of the total force at $0{\cdot}1\,m\,s^{-1}$ (lift calculation B) and as much as 92 % if F_b is assumed to be associated with changing angles to balance the forces over the cycle (lift calculation A). Johnson *et al.* (1972) estimated the negative buoyancy of squid at 4 % of mass but concluded that this was negligible, allowing them to model a squid as in Fig. 3A (also neglecting F_r and T_f). This now seems unjustifiable since, in the present analysis based on Fig. 3B, 30 % of the total force is required to balance a negative buoyancy equal to 3·3 % of mass, even at the highest speed. This is an exorbitant price to pay, but the alternatives are even worse. If the squid stored 0·011 kg of lipid at $930\,kg\,m^{-3}$ in its digestive gland to neutralize buoyancy, it would occupy 87 % of the usable mantle volume, dramatically reducing the efficiency of the jet cycle.

In fact, negative buoyancy is probably only a problem for squid confined in a tunnel or pool. Existing schemes for energy saving in negatively buoyant organisms based on vertical movements such as 'climb-and-glide' in fish (Weihs, 1973) and 'hop and sink' in zooplankton (Haury & Wiehs, 1976) do not apply directly to squid, but the present analysis provides a basis for similar economies in jet swimming. Such a scheme for squid is particularly attractive since their vertical movements are well documented (Roper & Young, 1975). Squid forced to swim horizontally must constantly adjust their angle of attack in all phases and use cross-flow to generate lift during the refilling phase, which increases drag. Nature lacks such restrictions, however, and squid normally move freely in three dimensions.

O'Dor (1988*b*) calculated the cost of transport for *L. opalescens* based on

oxygen consumption in a swim-tunnel using the equation $P = 0{\cdot}0276e^{3{\cdot}95u}$ to estimate power consumption (in watts, assuming $20\,kJ\,l\,O_2^{-1}$) at various speeds. On the same basis, resting power consumption is 0·025 W (O'Dor, 1982). These data allow a comparison of horizontal swimming with climb-and-glide swimming. If the drag on a gliding squid is $D = B\sin\theta$ (Weihs, 1973) and if this is comparable to $D_b + D_f$, a squid gliding down at 15° should travel at $0{\cdot}175\,m\,s^{-1}$. A 1 m vertical drop would cover 7·1 m horizontally, presumably with a power consumption equal to resting. If the squid climbs back up at 45° and $0{\cdot}3\,m\,s^{-1}$, it will average $0{\cdot}18\,m\,s^{-1}$ over the horizontal distance (about 1 body length s^{-1}, a reasonable and close to optimal cruising speed). While climbing, the flow will parallel the squid's body ($\theta = 0°$), and the resistance to motion will be as indicated in Fig. 3A; there should be no D_p, no D_i and no F_b associated with attitude control. The jet thrust used in horizontal swimming (Fig. 3B) to counter these forces can be applied directly to countering buoyant weight by directing the funnel down at an angle of 23° to the body. At this speed and angle the forces just balance, so that the cost of climbing at $0{\cdot}3\,m\,s^{-1}$ is equal to the cost of swimming horizontally at the same speed. However, negative buoyancy makes another free glide possible. The total power consumption swimming at $0{\cdot}18\,m\,s^{-1}$ horizontally is 0·056 W, but the average over the climb-and-glide cycle is 35 % less at 0·036 W. This would significantly increase the calculated range of squid migrations. The net cost of transport, excluding rest metabolism as Weihs (1973) did for calculations on fish, indicates climb-and-glide savings for squid of over 60 % compared with horizontal swimming.

These savings may be an overestimate, being based on the most pessimistic assessment of the cost of lift (lift calculation A, Table 2). However, no effort was made to optimize the angles used, and there would still be significant savings with the more optimistic assumption (lift calculation B, Table 2) that angular adjustments cost nothing. Detailed analysis of the economies of climb-and-glide swimming in squid should await direct measurements of the cost of vertical movement from telemetered pressure data (Webber & O'Dor, 1986) and data on actual patterns of vertical movement in nature. Telemetered pressures from horizontally swimming squid in a large pool were actually marginally *higher* than those in a tunnel at equivalent speeds (Webber & O'Dor, 1986), but this squid did not appear to climb-and-glide in the confines of the pool. The 'ground effect' (Blake, 1979) resulting from the proximity of the tunnel wall may reduce the cost of the vertical component of tunnel swimming. Weihs (1977) has shown that intermittent jetting can be more efficient than a continuous jet if large vortices are formed frequently, but this is even less important in squid, with small orifices and low frequencies, than in medusae (Daniel, 1983). However, this factor should be considered in future analyses of juvenile squid which have higher frequencies and relatively larger orifices.

The analysis of Johnson *et al.* (1972) was primarily concerned with the forces during the acceleration phase of a single jet cycle, and did not consider the cost of refilling, although Trueman (1975) does mention a predicted speed after 4–5 cycles

for a 0·35 kg ($l_t \approx 0{\cdot}4$ m) *L. vulgaris* of 3·5 m s^{-1} based on an extended analysis using their approach. Both five cycles of continued acceleration and the final speed seem high in comparison to the present analysis (although scaling effects have not yet been tested) and to observations on larger squid (Webber & O'Dor, 1986), probably because refilling forces are underestimated. For squid, the present estimates indicate that at 0·1 m s^{-1} only 3 % of the forces are related to refilling, but at higher speeds this approaches 20 %, a much higher proportion than that associated directly with acceleration of the animal *per se*, as Table 2 shows. Flow-induced negative pressures (Vogel, 1987) could aid in refilling at higher speeds in larger squid. The exact magnitude of refilling forces needs further study, but Gosline & Shadwick's (1983) data on the energy available from mantle 'springs' to power refilling are generally consistent with present calculations. They predict the available energy in the springs at various mantle radii (their fig. 5) and a recovery efficiency of 75 %. The calculated energy available at the end of phase 2 at the measured mantle radii in the present study is only about 50 % higher than the energy required to generate the refilling forces over phase 1 at the higher speeds. Thus, the refilling forces used are reasonable.

Although many volumes have been written about squid giant axons since Young's 1938 study, little is really known of what they do. Even the studies examining the role of the neuromuscular system in squid locomotion (Wilson, 1960; Packard & Trueman, 1974) have generally lacked information on normal swimming. The present observations only indicate indirectly how muscles act, but they do so for the type of swimming least studied and provide some insights. Packard & Trueman (1974) suggest that there are two populations of muscle fibres innervated by small and giant fibres responsible for respiratory and escape cycles, respectively. Two groups (Mommsen *et al.* 1981; Bone *et al.* 1981) have shown that squid mantles contain a layer of 'anaerobic' muscle fibres sandwiched between two layers of 'aerobic' fibres, but the innervation of these fibres remains unclear. Gosline *et al.* (1983) have, however, shown separate activity of radial fibres during hyperinflation implying a third type of innervation not yet identified anatomically. The muscle length changes reflected in the volume data in Fig. 2 suggest that the full range of mantle activity could be explained if the three layers of circular muscles and the radial muscles each received separate 'all-or-none' innervation without feedback. The low-amplitude mantle radius changes at 0·1 m s^{-1} are presumably what have been described as respiratory contractions and could be driven by one of the two layers of aerobic fibres. The greater contractions at higher subcritical speeds could involve the second layer, and the even stronger contractions at non-sustainable, supracritical speeds would require anaerobic fibres as well (O'Dor, 1988*b*). Escape jets, then, would differ from supracritical jets only in the added involvement of radial fibres producing hyperinflation. At intermediate speeds, variations in pressure and jet velocity appear to depend largely on changes in the funnel orifice. The increase in pressure and, therefore, tension during phase 2 by 40 % between 0·2 and 0·4 m s^{-1}, which should – but does not – affect the speed of shortening, may reflect the self-regulatory properties of obliquely striated

muscle (Rosenbluth, 1972; Kier, 1985). There is still much to be learned about the integrated neuromuscular responses in squid mantle.

The capacity for fine control of other motor systems has also been underestimated. Triggering of fin activity is independent of mantle contractions. Three clearly different modes of fin action can be identified in Fig. 2 with changing speed in a single style of swimming, and there are certainly many more. The funnel, too, is more than the simple directional nozzle of fixed cross-section assumed in earlier studies (Johnson *et al.* 1972). The pattern of increasing funnel radius at $0{\cdot}2\,m\,s^{-1}$ in Fig. 4 might simply result from stretching under pressure, but the best explanation for the increasing pressure with constant flow at higher speeds is active reduction of the maximum (or possibly average) funnel radius, as shown in Table 1. It is also difficult to explain the prolonged high pressures during an escape response unless funnel radius, as shown in Fig. 4, continues to decrease under active muscle tension. Squid may well have continuous dynamic control over the funnel orifice allowing them to optimize power output from a given volume change at a given speed, a relatively complex problem. When equation 7 is rewritten as $T_j = (d_w Q^2)/(\pi r_f^2)$, it is obvious that the same jet thrust can result from half as much volume change, if the funnel radius is also halved. Increasing thrust in this way, by increasing jet velocity, has a negative side, however. The jet's Froude efficiency (E, given in Table 1) depends on both squid speed, u, and jet velocity, u_j, $[E = u/(u+0{\cdot}5u_j)]$ (Alexander, 1977). If jet thrust at $0{\cdot}2\,m\,s^{-1}$ in Table 2 were achieved by halving the funnel radius, E would drop from 0·21 to 0·12, nearly doubling the power requirement. Fig. 4 certainly indicates that there is some sort of dynamic control. To optimize thrust and power the squid might regulate its funnel orifice in relation to its acceleration, which its statoliths can apparently measure (Stephens & Young, 1982). Squid use their complex nervous system to compensate for the inefficiency of jet propulsion (O'Dor & Webber, 1986), and it appears that we are only beginning to appreciate how sophisticated the control of mantle, funnel and fins is.

This work was funded by grants from the Natural Sciences and Engineering Research Council of Canada and Fisheries and Oceans Canada. The help and ideas of J. M. Gosline, R. W. Blake, J. Trotter and many other colleagues in the Zoology Department of the University of British Columbia where I was a Visiting Professor during the analytical phase are gratefully acknowledged. Thanks also to T. Daniel for advice, the staff of the Bamfield Marine Station who helped swim the squid, to K. Ottenbrite for recording much of the kinematic data and to E. Foy for a class project which first suggested the advantages of climb-and-glide.

References

ALEXANDER, R. McN. (1977). Swimming. In *Mechanics and Energetics of Animal Locomotion* (ed. R. McN. Alexander & G. Goldspink), pp. 222–248. London: Chapman & Hall.

BLAKE, R. W. (1979). The energetics of hovering in the Mandarin Fish (*Synchropus picturatus*). *J. exp. Biol.* **82**, 25–33.

BLAKE, R. W. (1980). Undulatory median fin propulsion of two teleosts with different modes of life. *Can. J. Zool.* **58**, 2116–2119.

BLAKE, R. W. (1983). *Fish Locomotion*, 208pp. Cambridge: Cambridge University Press.

BONE, Q., PULSFORD, A. & CHUBB, A. D. (1981). Squid mantle muscle. *J. mar. biol. Ass. U.K.* **61**, 327–342.

BRADBURY, H. E. & ALDRICH, F. A. (1969). Observations on locomotion of the short-finned squid, *Illex illecebrosus illecebrosus* (Lesueur, 1821), in captivity. *Can. J. Zool.* **47**, 741–744.

BRETT, J. R. (1964). The respiratory metabolism and swimming performance of young sockeye salmon. *J. Fish. Res. Bd Can.* **21**, 1183–1226.

DANIEL, T. L. (1983). Mechanics and energetics of medusan jet propulsion. *Can. J. Zool.* **61**, 1406–1420.

DANIEL, T. L. (1984). Unsteady aspects of locomotion. *Am. Zool.* **24**, 121–134.

DANIEL, T. L. (1985). Cost of locomotion: unsteady medusan swimming. *J. exp. Biol.* **119**, 149–164.

FREADMAN, M. A., HERNANDEZ, L. & SCHAROLD, J. (1984). Swimming biology of squid, *Loligo pealei. Am. Zool.* **24**, 123A.

GOSLINE, J. M. & DEMONT, M. E. (1985). Jet-propelled swimming in squids. *Scient. Am.* **252**, 96–103.

GOSLINE, J. M. & SHADWICK, R. E. (1983). The role of elastic energy storage mechanisms in swimming: an analysis of mantle elasticity in escape jetting in the squid, *Loligo opalescens. Can. J. Zool.* **61**, 1421–1431.

GOSLINE, J. M., STEEVES, J. D., HARMAN, A. D. & DEMONT, M. E. (1983). Patterns of circular and radial mantle muscle activity in respiration and jetting of the squid *Loligo opalescens. J. exp. Biol.* **104**, 97–109.

GRAY, J. (1933). Studies in animal locomotion. II. The relationship between waves of muscular contraction and the propulsive mechanism of the eel. *J. exp. Biol.* **10**, 386–390.

HAURY, L. & WEIHS, D. (1976). Energetically efficient swimming behaviour of negatively buoyant zooplankton. *Limnol. Oceanogr.* **21**, 797–803.

HERTEL, H. (1966). *Structure – Form – Movement.* pp. 223–224. New York: Reinhold.

HOERNER, S. F. (1965). *Fluid Dynamic Drag.* pp. 3.11–3.12. Published by the author.

JOHNSON, W., SODEN, P. D. & TRUEMAN, E. R. (1972). A study in jet propulsion: an analysis of the motion of the squid, *Loligo vulgaris. J. exp. Biol.* **56**, 155–165.

KIER, W. M. (1985). The musculature of squid arms and tentacles: ultrastructural evidence for functional differences. *J. Morph.* **185**, 223–239.

LAMB, H. (1962). *Hydrodynamics.* pp. 152–156. Cambridge: Cambridge University Press.

MAGNUSON, J. J. (1978). Locomotion by scombrid fishes: Hydromechanics, morphology and behaviour. In *Fish Physiology*, vol. 7 (ed. W. S. Hoar & D. J. Randall), pp. 240–315. London: Academic Press.

MOMMSEN, T. P., BALLANTYNE, J., MACDONALD, D., GOSLINE, J. & HOCHACHKA, P. W. (1981). Analogs of red and white muscle in squid mantle. *Proc. natn. Acad. Sci. U.S.A.* **78**, 3274–3278.

O'DOR, R. K. (1982). Respiratory metabolism and swimming performance of the squid, *Loligo opalescens. Can. J. Fish. aquat. Sci.* **39**, 580–587.

O'DOR, R. K. (1988*a*). The energetic limits on squid distributions. *Malacologia* **29**, 113–119.

O'DOR, R. K. (1988*b*). The limitations on squid performance. *J. appl. Physiol.* **64**, 128–134.

O'DOR, R. K. & WEBBER, D. M. (1986). The constraints on cephalopods: why squid aren't fish. *Can. J. Zool.* **64**, 1591–1605.

PACKARD, A. (1969). Jet propulsion and the giant fibre response in *Loligo. Nature, Lond.* **221**, 875–877.

PACKARD, A. & TRUEMAN, E. R. (1974). Muscular activity of the mantle of *Sepia* and *Loligo* (*Cephalopoda*) during respiratory movements and jetting, and its physiological interpretation. *J. exp. Biol.* **61**, 411–419.

ROPER, C. F. E. & YOUNG, R. E. (1975). Vertical distribution of pelagic cephalopods. *Smithson. Contrib. Zool.* **209**, 1–51.

ROSENBLUTH, J. (1972). Obliquely striated muscle. In *The Structure and Function of Muscle* (ed. G. H. Bourne), pp. 389–421. New York: Academic Press.

STEPHENS, P. R. & YOUNG, J. Z. (1982). The statocyst of the squid *Loligo*. *J. Zool., Lond.* **197**, 241–266.

TRUEMAN, E. R. (1975). *The Locomotion of Soft-Bodied Animals*. pp. 129–150. New York: American Elsevier Publishing Company, Inc.

TRUEMAN, E. R. (1980). Swimming by jet propulsion. In *Aspects of Animal Movement* (ed. H. Y. Elder & E. R. Trueman), pp. 93–105. Cambridge: Cambridge University Press.

TRUEMAN, E. R. & PACKARD, A. (1968). Motor performances of some cephalopods. *J. exp. Biol.* **49**, 495–507.

VOGEL, S. (1987). Flow-assisted mantle cavity refilling in jetting squid. *Biol. Bull. mar. biol. Lab., Woods Hole* **172**, 61–68.

WARD, D. V. & WAINWRIGHT, S. A. (1972). Locomotory aspects of squid mantle structure. *J. Zool., Lond.* **167**, 437–449.

WEBB, P. W. (1978). Hydrodynamics: Nonscombroid fish. In *Fish Physiology*, vol. 7 (ed. W. S. Hoar & D. J. Randall), pp. 190–239. London: Academic Press.

WEBBER, D. M. & O'DOR, R. K. (1986). Monitoring the metabolic rate and activity of free-swimming squid with telemetered jet pressure. *J. exp. Biol.* **126**, 205–224.

WEIHS, D. (1973). Mechanically efficient swimming techniques for fish with negative buoyancy. *J. mar. Res.* **31**, 194–209.

WEIHS, D. (1977). Periodic jet propulsion of aquatic creatures. In *Bewegungsphysiologie-Biomechanik* (ed. W. Nachtigal), pp. 171–175. Town: Publisher.

WILSON, D. M. (1960). Nervous control of movement in cephalopods. *J. exp. Biol.* **37**, 57–72.

YOUNG, J. Z. (1938). The functioning of the giant nerve fibres of the squid. *J. exp. Biol.* **15**, 170–185.

ZUEV, G. V. (1968). Characteristic features of the structure of cephalopod molluscs associated with controlled movements. *Fish. Res. Bd Can. Transl. Ser. no. 1011*.